Earth and Planetary Science Letters 284 (2009) 151–156

Contents lists available at ScienceDirect

Earth and Planetary Science Letters

journal homepage: www.elsevier.com/locate/epsl

Crater–fault interactions: A metric for dating fault zones on planetary surfaces

Matthew R. Smith *, Alan R. Gillespie, David R. Montgomery, J. Batbaatar

Department of Earth and Space Sciences, University of Washington, Seattle, WA 98195-1310, United States of America

ARTICLE INFO

Article history:
Received 9 December 2008
Received in revised form 3 April 2009
Accepted 15 April 2009
Available online 31 May 2009
Editor: T. Spohn

Keywords:
Mars
craters
impacts
chronology
tectonics
Thaumasia
techniques

ABSTRACT

Constructing a tectonic history of a planetary surface requires determining precise fault ages, a task not always possible with current analytical methods. Here we introduce a new method to constrain the ages of faults, improving upon earlier methods that used cross-cutting relationships with crater-dated host surfaces, and apply it to faulted terrains by counting all craters and categorizing them into "faulted," "unfaulted" and "unclear" types to date deformation directly. Additionally, we construct a simple probabilistic model to account for regions of low fault density. This new technique is applied to the tectonically complex Thaumasia plateau, Mars, to assess the timing of regional faulting and demonstrate its usefulness and ease of application.

1. Introduction

Previous studies that have dated faulting events on planetary surfaces have relied on the geologic principle of cross-cutting relationships to constrain their range of possible ages (e.g. Wise et al., 1979, Plescia and Saunders, 1982; Dohm and Tanaka, 1999). Surfaces that are cut by faults must be older than the faults they host; if a fault encounters a surface and does not cut it, the surface age must be younger than the fault. The ages of the fault-adjacent surfaces may be determined through crater densities, from which a range of possible ages for the faulting event may be deduced. This technique has been employed successfully but requires two conditions for precise age estimates: the fault must encounter surfaces both older and younger than the faulting, and the difference in age between the two surfaces must be small. If either condition is not met, the precision of the age determination for that fault is reduced commensurately.

A technique to improve precision was devised by Tanaka (1982) based on the interaction between the age of a linear feature, or sets of linear features – such as faults, ridges, and channels – and the craters they cross. An area enveloping the linear feature is surveyed for crater density and crater–feature relationships. If the linear feature does not affect a crater, it is assumed to predate the crater. If it cuts through the crater, the crater is assumed to have formed first. The population of craters which post-date the feature can then be used to date its formation directly. This technique has been previously employed by Wichman and Schultz (1986) to study coarse-scale martian extensional tectonics and has been recently used by Fassett and Head (2008) to determine the age of martian valley networks. However, applications of this method are restricted to areas with low densities of linear features, since high densities result in overlapping survey areas between adjacent features and time-intensive surveys of several individual features.

A variation on this technique was also described by Mangold et al. (2000), which studied the interaction between craters and compressional ridges. They determined the range of ages of faulting events by counting craters not located on faults – meaning they have no relationship to the deformation – and used them to determine the upper age limit for deformation. The lower age constraint was still provided by an adjacent surface which must bury a portion of the ridge, thereby post-dating its formation.

The purpose of this paper is to extend earlier techniques to areas with high densities of linear features. We achieve this by counting all craters over a surface and categorizing them according to their relationship to the features being studied. Throughout this article, we will discuss this new technique mainly in the context of extensional fault zones, these being common high-density linear features on planetary surfaces, but this technique may also be applied to other linear features, such as dense valley networks and dike swarms. In the absence of high fault densities, we have also devised a simple probabilistic model to be applied to crater counts to compensate for

* Corresponding author. Tel.: +1 206 543 4914.
E-mail address: matthers@u.washington.edu (M.R. Smith).

0012-821X/$ – see front matter
doi:10.1016/j.epsl.2009.04.025

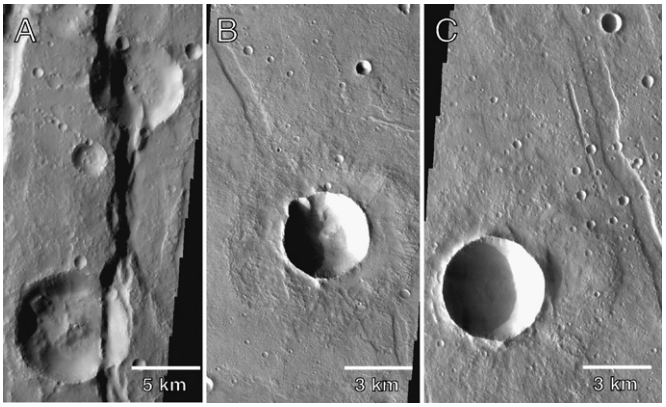

Fig. 1. Examples of crater–fault relationships. A) Craters cut by faults (V09928003); B) large crater superposing faults (V15344003). Pre-existing grabens can be seen draped by the crater ejecta; C) crater not directly on a fault, with unclear age relationship with faulting (V14820005).

few craters interacting with faults. We thus determine deformation ages for surfaces with a wide range of densities of surface features.

2. Technique

To assess the age of the faulting, we count craters on the entire faulted surface, separating the crater population into those that superpose and post-date the faults and those that are cut by them (Fig. 1). If a crater is not located on a fault, it is classified into a third category of unknown age relationship. The unfaulted crater population by itself provides the lower bound on the age determination; the combined unfaulted and unclear crater populations provide the corresponding upper bound. Fault interactions with ejecta blankets are not considered in this study, since whether ejecta are cut by or drape a fault is not easily determined in satellite images. A MOLA topographic cross-section across an ejecta-draped fault may reveal diagnostic subdued topography but is not necessarily conclusive, since MOLA footprints are often too large for narrow faults. A threshold minimum diameter for counted craters should be chosen, proportional to the average spacing of faults in order to increase the likelihood that all counted craters will encounter a fault. For regions of lower fault densities, a correction is applied as described in Section 2.1.

The population of craters that post-date fault formation is then compared to the crater-defined stratigraphic time-units as established by Tanaka (1986) to assess relative age. Numeric ages are estimated by comparing binned counts to lunar-derived isochrons, as described by Hartmann (2005). By isolating those craters which encounter faults but are unfaulted – indicating that they have formed after faulting terminated – we can calculate the amount of time passed since the cessation of faulting. The advantage of this technique is direct dating of the deformation age with crater statistics, rather than surface ages.

2.1. Data correction for low fault density

Surfaces with low fault densities make comprehensive crater counting more difficult, since a large fraction of small craters lie between the widely spaced faults, reducing the number of craters that help to constrain the timing of faulting. We have therefore constructed a simple probabilistic model to estimate the population of craters that would have had the opportunity to be faulted, had faults been more closely spaced, so that we may apply that estimate to adjust the crater counts.

The probability, P, of a single N–S trending fault, cutting through a defined survey area of size $L \times L$ that contains a single crater of diameter D and not encountering it is given as:

$$P(D) = \frac{L - D}{L}. \tag{1}$$

To define the probability P_U that the same crater is missed by all faults that cut through the same area, we must include a term, as an exponent, for the number of faults, F:

$$P_U(D) = \left(\frac{L-D}{L}\right)^F. \tag{2}$$

Therefore, the probability P_F of a single crater being faulted from a given number of parallel faults cutting through our survey area is given by:

$$P_F(D) = 1 - \left(\frac{L-D}{L}\right)^F. \tag{3}$$

The average number of faults, F, may be estimated by calculating the net fault length within a sample area and dividing it by the surveyed area to determine a number of faults per unit area. The measured crater abundances in a target area may then be divided by $P_F(D)$ to correct for the unlikelihood of a crater within a given diameter range to encounter a fault and contribute to our measurements.

3. Application: Thaumasia plateau, Mars

As a case study, we applied our technique to the Thaumasia plateau, a region with a complex faulting history. There are several heavily deformed regions that form the edges of the plateau and display a dense network of extensional faults, and areas to the south of the plateau which exhibit less dense faulting and can serve as an application of our correction for low fault densities.

3.1. Context

The Thaumasia plateau is a volcano-tectonic province located southeast of the Tharsis volcanic complex (Fig. 2). It records a tectonically active past, with several heavily faulted areas resulting from different regional stress regimes (Dohm and Tanaka, 1999). Compressional strain along the Thaumasia highlands and the Coprates rise formed a large (~1–2 km high) frontal bulge and thrust faults that border the plateau (Schultz and Tanaka, 1994). Additional minor compression is expressed in concentric wrinkle ridges oriented circumferentially to Syria Planum. These ridges occur throughout the interior of the plateau and deform Hesperian lava flows. Widespread extension is expressed in the extensive and densely packed N–S transtensional grabens in Claritas Fossae, with fewer grabens located within the Thaumasia highlands and Melas Fossae, and also in Thaumasia Fossae. Extensional faults cut through mostly Noachian-aged rocks with some minor exposures of Hesperian-aged rock units in Claritas Fossae and the Thaumasia highlands (Dohm and Tanaka, 1999). The northern border of the plateau, Valles Marineris, originated as an area of extensional strain before being subsequently widened by an array of proposed mechanisms.

The formation of the regional grabens, some of which are oriented radially to volcanic centers within the Tharsis complex, has previously been interpreted as a result of volcanic loading (e.g. Solomon and Head, 1982), Tharsis uplift (e.g. Carr, 1973; Wise et al., 1979), or some combination of both (e.g. Banerdt et al., 1982). Alternatively, Montgomery et al. (2009) recently proposed that the tectonic history of the Thaumasia plateau suggests its evolution as a gravity slide and

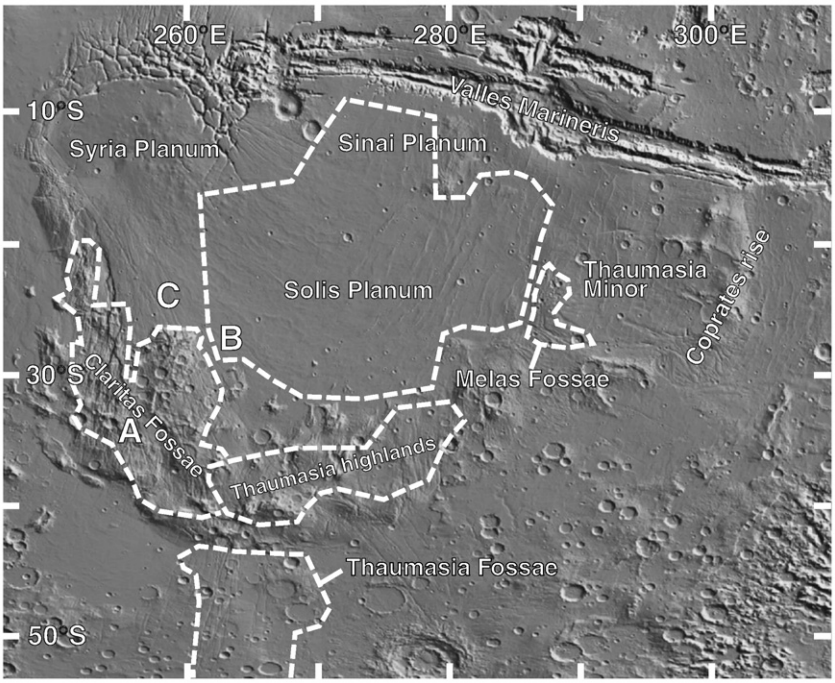

Fig. 2. Context map showing Thaumasia plateau (bordered by Claritas Fossae to the west, Thaumasia highlands to the south, Coprates rise to the east, and Valles Marineris to the north) and vicinity. Dashed lines indicate the extent of areas surveyed for this study. A–C indicate locations of examples in Fig. 1.

that Claritas Fossae resembles a trailing imbricate extensional fan, a tectonic feature common in terrestrial regions of gravitational spreading.

The timing of faulting near the Thaumasia plateau has been previously estimated from cross-cutting relationships between the fault systems and their host surfaces that have been dated using crater counts. Faulting at Thaumasia has been estimated to occur in four to six stages (Plescia and Saunders, 1982; Tanaka and Davis, 1988; Dohm and Tanaka, 1999; Anderson et al., 2001), with many of these stages separated by a shift in the center of radial faulting or a period of intense volcanism or both. Most models of faulting either explicitly or implicitly require that regional faulting persisted for much of the Noachian and Hesperian periods. The gravity-slide hypothesis of Montgomery et al. (2009) suggests two stages of faulting, separated by an undetermined amount of time. The first stage involves deformation of the Thaumasia highlands and Coprates rise resulting from large-scale gravity-driven movement of the Thaumasia plateau to the southeast. The second stage involves the movement of a smaller eastern block on the plateau, called Thaumasia Minor (Thaumasia Planum), which is bordered by Melas Fossae to the west and Coprates rise to the east. The formation of Valles Marineris and wrinkle ridges on the interior of the plateau is also posited to have occurred during the second stage of activity.

3.2. Analysis

We applied our new technique of dating faulted regions to the areas denoted in Fig. 2. Marked regions represent the surveyed locations, not the full extent of the feature. Areas were selected for high fault abundance and uniformity of fault densities.

Initial crater counts were performed on a 1/128°-resolution MOLA-derived shaded relief map, with fault–crater superposition relationships verified with THEMIS-VIS and IR images. For this study, we chose our threshold minimum crater diameter as 5 km, since smaller craters often would fall between faults and definitive crater–fault relationships could not be determined. Crater counts, not considering any deformation, were also performed on Solis and Sinai plana for correlation with ages of faulting. Counting statistics are given in Table 1.

In Thaumasia Fossae, fault density is lower than in the other surveyed regions. Therefore, we applied our data correction to account for the higher percentage of craters that did not happen to encounter a fault. For this correction, we calculated the fault density by tracing all faults within the Thaumasia Fossae survey area using GIS software to compute a net fault length of 8210 km, and divided by our surveyed area, 231,714 km^2, to compute an average fault density per unit area: thirty five 1000-km faults per 10^6 km^2. We then divided our measured crater abundances at Thaumasia Fossae by the probability distribution, $P_F(D)$, to correct for the unlikelihood of a crater within a given diameter range to encounter a fault and contribute to our measurements. To validate this correction, we also performed the low fault-density buffered crater-counting technique of Tanaka (1982) for comparison and found that the populations of buffered and corrected

Table 1
Crater counting statistics for surveyed areas.

Location	Area (km^2)	No. faulted craters	No. unfaulted craters	No. indeterminate craters	Total no. craters
Thaumasia Fossae	231,714	34	27	58	119
Thaumasia highlands	212,167	15	34	21	70
Melas Fossae	40,175	5	11	16	32
Claritas Fossae	405,027	68	135	48	251

Table 2
Martian time-unit periods and numeric ages for faulting in study areas.

Location	Age of termination of faulting	
	Time-unit age[a]	Numeric age[b] (Ga)
Thaumasia Fossae	LN	3.6
Thaumasia highlands	LN-EH	3.6–3.7
Melas Fossae	LN-EH	2.5–3.5
Claritas Fossae	LN-LH	2.5–3.3
Solis/Sinai plana	EH-LH	2.8[c]

LN = Late Noachian, EH = Early Hesperian, LH = Late Hesperian.
[a] Derived from the chronology of Tanaka (1986).
[b] Derived from the chronology of Hartmann (2005).
[c] Age of surface, not of faulting.

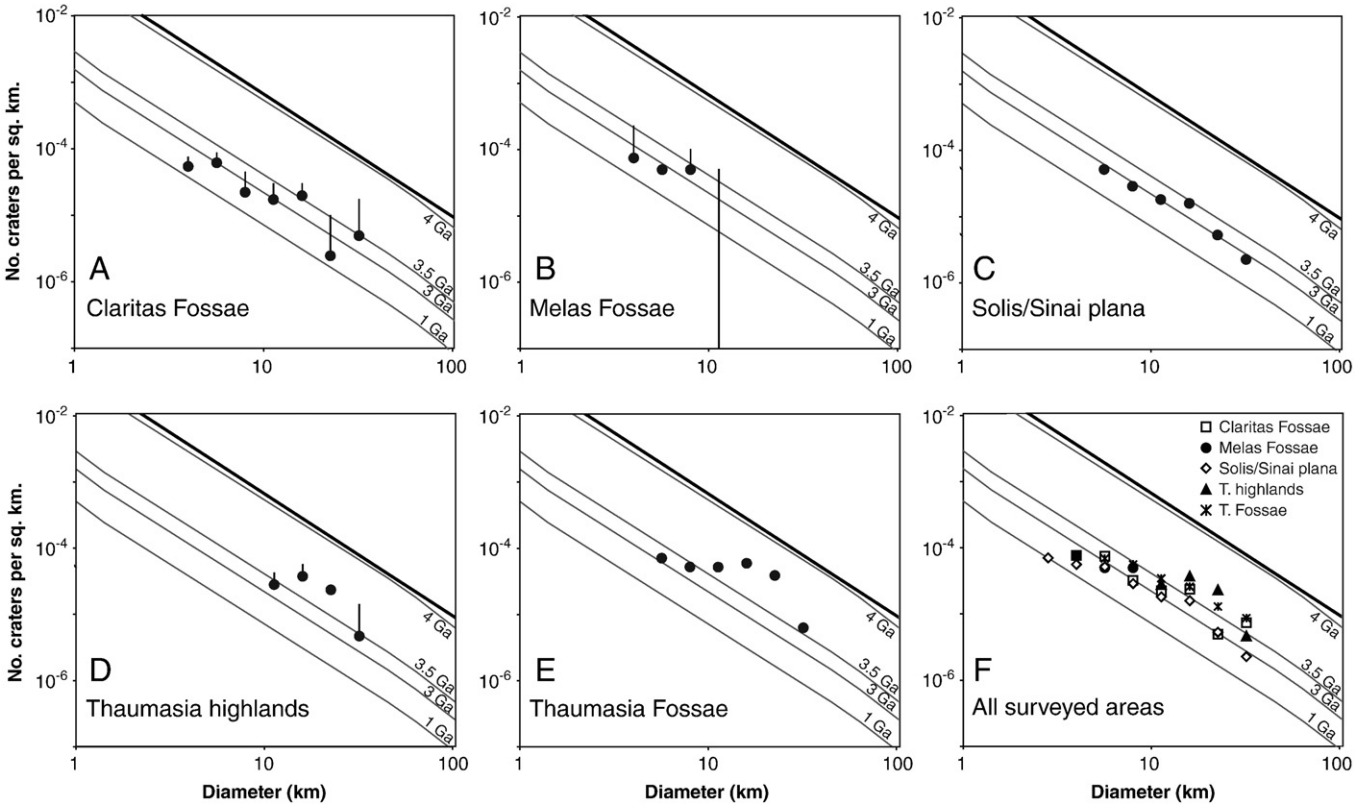

Fig. 3. Crater-count plots depicting abundances of craters that superpose faults (those that have formed since termination of faulting). Bars indicate range of possible values including craters with unclear relationship with faulting.

craters are statistically similar with 95% confidence utilizing the χ^2 similarity test, a statistical measure of similarity of binned data. Average crater abundances ($D>5$ km) per square kilometer are given as follows: unfaulted (+ unclear) -9.49×10^{-5} (3.11×10^{-4}), corrected counts (as described in this study) -2.8×10^{-4}, and buffered crater counts (from the technique of Tanaka, 1982) -1.61×10^{-4}. Overall, our correction results in a higher number of smaller craters being assigned as unfaulted or faulted, while the number of larger craters that are categorized as unfaulted or faulted changes very little, since they are large enough to have encountered a fault prior to the correction.

3.3. Results

Time unit assignments according to cumulative crater abundances, derived from the chronology of Tanaka (1986), are shown in Table 2. All ages, except for Thaumasia Fossae and Solis/Sinai plana, are ascertained using the uncorrected crater counts. Corrected counts vary negligibly from the uncorrected counts in these areas since fault densities are very high and spacing between faults is very narrow. Crater abundances were binned according to diameter, as described by Hartmann (2005) and plotted in Fig. 3. A best-fit isochron, from which an approximate age was derived, was measured using linear regression of log-transformed data (Table 2). To evaluate the systematic error in our counts, we performed two independent counts of a large portion of our Claritas Fossae survey area. Comparison showed that the average error measurement between counts was 20%, which is less than the range defined by our unfaulted and unfaulted + unclear populations (~33%). Therefore, we are confident that the systematic error does not meaningfully alter our results.

Fig. 4 depicts all crater counts for Claritas Fossae, including unfaulted, faulted and total craters for the region. Claritas Fossae is mainly composed of Noachian-aged geologic units, with little local variability in surface ages to help constrain the ages of faults. This complication is noted by Dohm and Tanaka (1999) in their assessment of the ages of tectonic features in the Thaumasia region and was rectified by extrapolating fault relationships from similarly oriented faults elsewhere where differently aged surfaces are present. In the absence of two nearby surfaces to provide upper and lower limits on the age of faults, the only direct constraints of deformation age are provided by surface ages. Fig. 4 displays the difference between surface and deformation ages. The total crater count demonstrates a surface age of 3.7–3.9 Ga, which would provide only an upper limit on the deformation age. However, the uncorrected population of unfaulted craters, which represents the age of deformation, gives a much younger age of 2.5–3.3 Ga. By isolating craters according to their

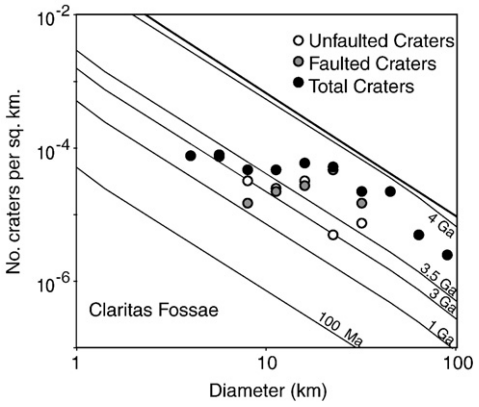

Fig. 4. Crater-count plot for Claritas Fossae. Includes counts for unfaulted, faulted, and total craters.

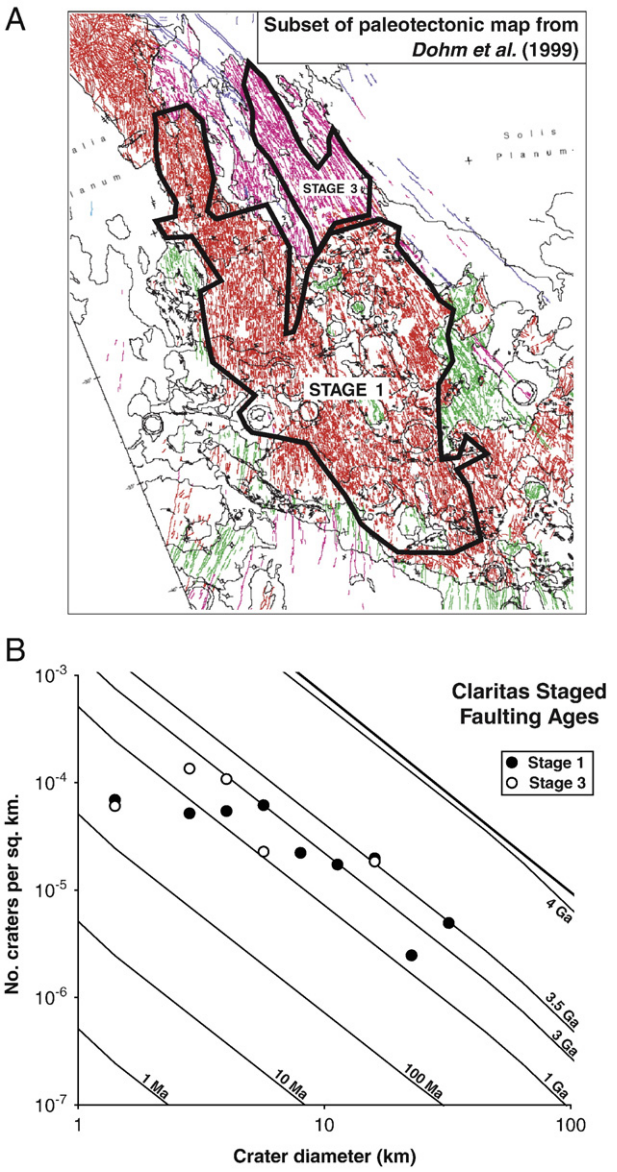

Fig. 5. Age comparison of Stage 1 and 3 faulting events. A) Subset of Thaumasia plateau paleotectonic map with designated Stage 1 and 3 survey areas (modified from Dohm et al., 2001); B) crater-count plot representing those craters which superpose and post-date faults in Stages 1 and 3.

relationship with the studied deformation, we can better constrain the age of faulting.

From our counts of unfaulted craters, we can establish a regional deformation timeline. The oldest event appears to be the faulting episode at Thaumasia Fossae, which is restricted to the Late Noachian period. However, this faulting may be roughly contemporaneous with the extensional faulting in the Thaumasia highlands, which appears younger according to the chronology of Tanaka (1986), but roughly coeval using the isochrons of Hartmann (2005). Other events – faulting at Claritas Fossae and Melas Fossae and the formation of the surface at Solis/Sinai Planum – appear younger than faulting at the Thaumasia highlands and Thaumasia Fossae and coeval within the margin of error of our data. Age data permit an event separation of as much as ~1 Ga or as little as zero time between the two stages of faulting.

The two phases of deformation are confirmed through statistical analysis using a χ^2 similarity test of binned crater-count data. With 95% confidence, we find that the populations of unfaulted craters at the Thaumasia highlands and Thaumasia Fossae are statistically similar, as are those at Claritas Fossae, Melas Fossae, and Solis/Sinai plana. However, the two groups are dissimilar from each other. The only exception is Melas Fossae, which appears statistically similar to the Thaumasia highlands rifts, perhaps due to a sparse crater population at Melas Fossae, which weakens the discriminating power of χ^2 testing.

An important comment on these results is that most of our crater counts do not happen to fall along a single isochron, as might be expected for a surface, or event, of a single age. However, deviations from isochrons are common on ancient surfaces and have been described since the formulation of crater-derived dating (e.g., Öpik, 1966; Hartmann, 1971). Crater loss over time is expected on Noachian and Hesperian-aged surfaces and has been attributed to slow, persistent processes such as long-term aeolian modification (e.g., Smith et al., 2008) or impulsive processes such as burial by thin lava flows (Hartmann et al., 1981). Both processes act to remove craters at small diameters preferentially, leaving the larger, more resilient craters to use for dating purposes.

3.4. Discussion

The results of this study point to two statistically distinct stages of deformation of the Thaumasia plateau, with stages separated by ~0–1 Ga. This general sequence is a departure from previous models of the tectonic evolution of the region, which supposed four to six distinct stages of faulting. This finding is a direct consequence of the improved analytical method introduced here, which can be used to ascertain a narrower range of possible deformation ages. The additional possibility that the two stages of faulting may have themselves been nearly coeval, perhaps equivalent to one extended period of regional tectonic activity, reveals that faulting here may have been much more temporally restricted and less episodic than originally estimated.

Previous studies which provided detailed geologic and tectonic maps of the Thaumasia plateau have been extensive in their scope and level of detail, and have revealed a complex co-evolution of tectonism, volcanism and hydrologic activity. Our case study does not dispute their findings of multiple stages of tectonic activity.

We reconcile our one- or two-staged faulting history with previous studies, specifically the most recent work performed by Dohm and Tanaka (1999) which described as many as five stages of faulting, by requiring their timeline of events to be more temporally restricted than previously estimated. We justify this explanation in two ways. First, we isolate their Stages 1–3 (Noachian to mid-Hesperian) from Stages 4 and 5 (Late Hesperian to Amazonian), as defined by Dohm and Tanaka (1999), since Stages 4 and 5 constitute a minor portion of the Thaumasia fault population with 1–2% and 0.1%, respectively. The faults within Stages 4 and 5 are also not found in close association with the major fault systems of Stages 1–3, and are described as most likely formed from stresses induced by the formation of the younger Tharsis Montes or by minor late-stage volcanism at Syria Planum. Therefore, we exclude Stages 4 and 5 from the discussion of the major tectonic evolution of the Thaumasia plateau, which is commonly associated with major activity of Syria Planum. With this in mind, we observe that each of the tectonic complexes associated with the major phase of activity in Thaumasia (Thaumasia highland rifts and Claritas, Thaumasia, and Melas Fossae) spans Stages 1 through 3. Furthermore, since there is no way to determine the age of the onset of tectonic activity besides the constraints offered by the age of the host rock, the deformation of Noachian rocks ascribed to Stage 1 may possibly be Hesperian-aged and associated with Stages 2 or 3. This uncertainty of onset age is noted by Dohm and Tanaka (1999) and justified by a higher density of faults in Noachian rock units (Stage 1) than in the younger Hesperian units, indicating that Stage 1 represented an early and distinct period of intense faulting. However, the large number of faults in Noachian units may also be explained through strain localization in older and weaker Noachian units or concentrations of faulting along the edges of a gravity slide, as proposed by Montgomery et al. (2009). Therefore, the majority of Thaumasia tectonism may

have been temporally restricted to a narrower period of time in the Late Noachian or Early Hesperian.

The second line of evidence for our new timeline is gained from an additional test which determines the temporal separation between Stages 1 and 3. We employed our method of crater–fault interaction dating once again on two adjacent surfaces in Claritas Fossae: one containing deformation ascribed to Stage 1 and the other to Stage 3. The results are given in Fig. 5. From the crater-count data, we find that the deformation ages in Stages 1 and 3 are indistinguishable, thereby suggesting further that Stages 1–3 may have occurred over a much shorter interval of time than previously believed, and indeed may have been roughly coeval. Uncertainty in crater counts is assumed to be equal to the systematic error as determined previously (~20%). We note that while neither set of crater counts follows a predicted isochron, both of our surveyed regions are older than 3 Ga and have been subjected to considerable post-emplacement modification, which would result in a characteristic crater population which deviates from isochrons at smaller diameters (e.g., Hartmann, 1971; Smith et al., 2008), as observed.

Our calculated sequence of events is consistent with the one or two stages of deformation proposed by Montgomery et al. (2009) for the gravity-slide model of faulting in Thaumasia. Our calculations from this study and their hypothesized timeline agree that faulting began in the south, by first deforming the Thaumasia highlands, and progressed elsewhere, with Melas Fossae forming in the second pulse of tectonic activity.

A limit of our technique is that it can only directly calculate the amount of time which has passed since faulting ended, and not the duration of faulting. Unfortunately, ages of fault initiation are difficult to assess, since faults cut through all older terrain and there is no simple way to constrain the duration of faulting. Furthermore, faults restricted to Noachian units, including a majority of those counted for this study, may be much younger than the surface they deform.

The dearth of craters superposed by some faults and cut by others indicates that very few craters appear to have formed during faulting and thus that active faulting at these locations did not persist for long. This would contradict the theories of fault formation that require sustained faulting for much of the Noachian and Hesperian periods and across several stages of volcano formation. However, prolonged periods of faulting could be justified by invoking reactivation of previous faults, which would appear to have purely post-dated crater formation, despite a more complex crater–fault relationship.

4. Conclusions

We introduce a new technique to ascertain the formation ages of dense linear features more directly than possible previously, since it may be used to determine the age of deformation, rather than indirectly via the ages of host surfaces. With the inclusion of a probabilistic model for correction for surfaces with lower densities of features, this technique can be applied to several types of features of interest for planetary scientists, including in tectonic and fluvial terrains.

Acknowledgment

Participation of ARG was supported by NASA's MDAP grant NNX07AV77G.

References

Anderson, R.C., et al., 2001. Primary centers and secondary concentrations of tectonic activity through time in the western hemisphere of Mars. J. Geophys. Res. 106, 20,563–20,585.
Banerdt, W.B., Phillips, R.J., Sleep, N.H., Saunders, R.S., 1982. Thick shell tectonics on one-plate planets: applications to Mars. J. Geophys. Res. 87, 9723–9733.
Carr, M.H., 1973. Volcanism on Mars. J. Geophys. Res. 78, 4049–4062.
Dohm, J.M., Tanaka, K.L., 1999. Geology of the Thaumasia region, Mars: plateau development, valley origins, and magmatic evolution. Planet. Space Sci. 47, 411–431.
Dohm, J.M., Tanaka, K.L., Hare, T.M., 2001. Geologic map of the Thaumasia region of Mars. USGS Misc. Inv. Ser. Map I-2650 (scale 1:5,000,000).
Fassett, C.I., Head, J.W., 2008. The timing of martian valley network activity: constraints from buffered crater counting. Icarus 195 (1), 61–89.
Hartmann, W.K., 1971. Martian cratering III: theory of crater obliteration. Icarus 15, 410–428.
Hartmann, W.K., 2005. Martian cratering 8: isochron refinement and the chronology of Mars. Icarus 174, 294–320.
Hartmann, W.K., et al., 1981. Chronology of planetary volcanism by comparative studies of planetary cratering. In: Merrill, R., Ridings, R. (Eds.), Basaltic Volcanism on the Terrestrial Planets. Pergamon Press, New York, pp. 1050–1127.
Mangold, N., et al., 2000. Chronology of compressional deformation on Mars: evidence for a single and global origin. Planet. Space Sci. 48, 1201–1211.
Montgomery, D.R. et al., 2009. Continental-scale salt tectonics on Mars and the origin of Valles Marineris and associated outflow channels. Geol. Soc. Am. Bull. 121 (1–2), 117–133. doi:10.1130/B26307.1.
Öpik, E.J., 1966. The martian surface. Science 153, 255–265.
Plescia, J.B., Saunders, R.S., 1982. Tectonic history of the Tharsis region, Mars. J. Geophys. Res. 87, 9775–9791.
Schultz, R.A., Tanaka, K.L., 1994. Lithospheric-scale buckling and thrust structures on Mars: the Coprates rise and south Tharsis ridge belt. J. Geophys. Res. 99, 8371–8385.
Smith, M.R., Gillespie, A.R., Montgomery, D.R., 2008. The effect of obliteration on crater-count chronologies for martian surfaces. Geophys. Res. Lett. 35, L10202.
Solomon, S.C., Head, J.W., 1982. Evolution of the Tharsis province of Mars: the importance of heterogeneous lithospheric thickness and volcanic construction. J. Geophys. Res. 87, 9755–9774.
Tanaka, K.L., 1982. A new time-saving crater-count technique, with applications to narrow features (abstract). Reports on Planetary Geology Program, NASA Tech. Memo. TM 35127, pp. 123–125.
Tanaka, K.L., 1986. The stratigraphy of Mars. J. Geophys. Res. 91, E139–E158.
Tanaka, K.L., Davis, P.A., 1988. Tectonic history of the Syria Planum province of Mars. J. Geophys. Res. 93 (B12), 14,893–14,917.
Wichman, R., Schultz, P.H., 1986. Timing of ancient extensional tectonic features on Mars (abstract). Lunar Planet. Sci. Conf. XVII, 942–943.
Wise, D.U., Golombek, M.P., McGill, G.E., 1979. Tharsis province of Mars: geologic sequence, geometry, and a deformation mechanism. Icarus 38, 456–472.